3D roof model generation and analysis supporting solar system positioning

3D roof model generation and analysis supporting solar system positioning

Filiberto Chiabrando[1], Chiara Danna[2], Andrea Lingua[2], Francesca Noardo[2], Anna Osello[3]

[1] Politecnico di Torino - DAD, viale Mattioli, 39 10125 Torino

[2] Politecnico di Torino - DIATI, c.so Duca degli Abruzzi, 24 10129 Torino

[3] Politecnico di Torino - DISEG, c.so Duca degli Abruzzi, 24 10129 Torino

filiberto.chiabrando@polito.it, chiara.danna@polito.it, andrea.lingua@polito.it, francesca.noardo@polito.it, anna.osello@polito.it

Abstract

Given the growing needs of renewable energy in urban areas, identifying suitable installation locations for solar systems is increasingly important. Existing energetic cadastres have often a limited level of detail in the analysed geometry, which needs to be rapidly updated following any changes in the buildings. The required 3D data can be generated by photogrammetry techniques and Structure-from-Motion (SfM) software. In this paper, the method was tested employing Digital Mapping Camera images (virtual images), on a case study in north-west of Italy. The results were analysed for assessing the reliability of the DSM produced by SfM methods, to be employed in solar radiation analyses. The problem of this kind of automatic 3D modelling could be sometimes the excessive detail in reconstructing the geometry of the roofs or the possible noise. The results are managed and analysed through Geographical Information System (GIS) tools. For the whole workflow, proprietary and free open source software (OSS) were used. The problems and limitations were investigated in order to evaluate and confirm the reliability and cost effectiveness of the described methods.

Keywords: Photogrammetry, structure-from-motion, open source, solar irradiation, GIS, surface analysis, DSM.

1. INTRODUCTION

The use of energy from renewable sources, in particular solar energy, is very challenging in urban environments, where the density of buildings is very high, and few surfaces are available. A key issue, for both private and public investors, is to identify and analyse surfaces best suited for the installation of photovoltaic or solar systems. Since the operators planning these activities are often professionals or administrators with different competences, a system that provides reliable results in an automatic or semi-automatic way could play a key role. Geomatics methods can be effective for this aim.

For the mapping of solar radiation, GIS (Geographical Information System) tools are an actual solution (Borfecchia et al., 2013, Hofierka et al., 2014), as demonstrated by the solar cadastres in some cities (for example New York, Boston, Bolzano, Morgex), available on the web. However, these services are limited in the level of detail of the roof analysis because they sometimes do not evaluate the real surface available nor the possible presence of obstacles on the roofs, such as dormers and chimneys. This deficiency is due to the fact that these applications consider rather large geographical areas and may not exploit the most appropriate

information. Even when LiDAR information is available, it often does not extract a dense three-dimensional representation, since generally the resolution is too low to acquire all the necessary details (Borfecchia et al., 2013). For example, the maximum density for a scale 1:2000 point cloud is usually 1 point every 0.80 m, which is not enough to capture all the useful details.

Other studies have employed photogrammetric systems for reconstructing detailed 3D models of buildings (Agugiaro et al., 2012). However, in this study, a very particular case is considered, since images acquired by a DMC (Digital Mapping Camera) are available, which are not usually processed in recent automatic software. It is a critical issue, even if the Structure from Motion (SfM) technique is nowadays well affirmed. In fact, it is usually employed to process close range images or common aerial images, which can have major distortions but a simpler geometry, since they are not the result of a composition of many images.

Once a suitable and accurate 3D representation of the roofs is achieved, which are usually the most available surfaces for solar panel installation in urban environments, their surfaces are analysed by solar radiation GIS tools. The results are validated by a comparison with the norm values for the geographical location considered. Moreover, a deeper analysis of the raster maps extracted by the DSM and critical to compute the received solar radiation (aspect and slope) is performed, in order to verify the reliability of the generated DSM by SfM technique, to be used for supporting solar radiation analyses. A summary of the phases is reported in Figure 1.

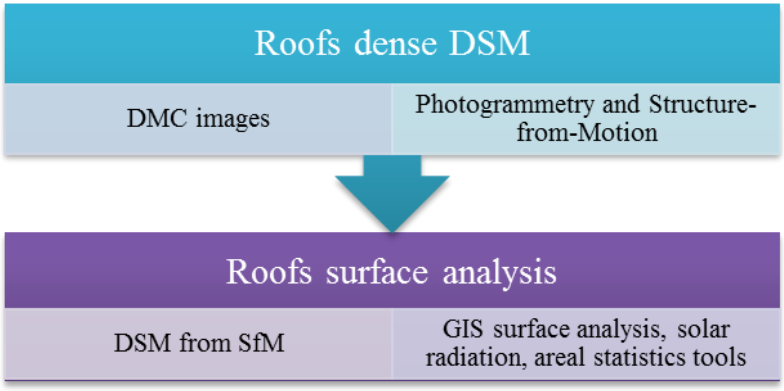

Figure 1: Flow-chart showing progress from DMC images to the 3D roof analysis.

The first objectives of this research is, therefore, the validation and test of the SfM technique employing DMC images.

Secondly, the analysis of the obtained 3D surfaces of the roofs is a central purpose of this study, to evaluate the reliability of the information extracted from them (slope, aspect, solar radiation information), notwithstanding the possible noise affecting some SfM products (due to the high level of detail, remaining outliers or simple noise effects). Some tests varying the computed values are performed, and some statistics are computed in order to assess the accuracies threshold in the surface analysis products. This permits the validation of the method to be used for cost and time effective mapping and analysis.

For each step in the study, we used open source software (OSS). The OSS proposes suitable tools to promote the sharing and exchange of data and information. OSS has two main advantages compared to proprietary software, which is important both for public administrations that need to respect the instructions, for example, in the Italian Circular 63/2013 (Agenzia per l'Italia Digitale, 2013), and also for private companies. Firstly, OSS saves on expensive licensing and maintenance costs, and also promotes the data interoperability by using open formats and implementing international standards. Secondly, the knowledge of the source code is a key element for effectively monitoring and controlling the software. This enables the user to adapt

the processing to specific needs and, where necessary, to correct, change or enhance the software itself, thus contributing to its improvement.

The test site considered in this paper is an area of Turin (north-west Italy) analysed during the DIMMER Project (District Information Modeling and Management for Energy Reduction). DIMMER is an EU project of the Seventh Framework Program for research and technological development set up in Manchester and Turin. In this project (2013/2016), industries, research centres and universities were involved, including the Politecnico di Torino, where the authors of this paper conduct their research. The aim of DIMMER was to realize an open platform for real time data processing, visualization and monitoring of energy consumption and production from renewable sources. In this paper, the proposed semiautomatic method for the generation of a 3D model of an area of Turin for supporting solar systems installation is described. Moreover, the data analysis in a GIS platform is also reported.

2. THE ROOF GEOMETRY MEASUREMENT AND RECONSTRUCTION: PHOTOGRAMMETRY AND SFM

The first objective was to generate a suitable 3D model of the roofs in the area using a photogrammetric approach. Existing images were used to realize a traditional photogrammetric plotting (vector map). The results of the manual plotting were compared with the results obtained using more automatic digital photogrammetry, Structure from Motion (SfM) and dense matching software tools.

The test area (approximately 0.2 km^2) was in the "Crocetta" district in Turin (Figure 2). The terrain is quite flat, but the buildings present different sizes and geometries.

Figure 2: Google map of the study area

The initial data consisted of 10 aerial images acquired in 2007 for an orthophoto map of Piemonte (the Region where Turin is located), from a flight height of about 900 m, permitting nominal scale of 1:2000: 0.40 m for both plane (tolerance 0.69 m) and height (tolerance 0.80 m) accuracy (Brovelli et al., 2010). The GSD of such images, considered the flight height and the pixel dimension, is 0.09 m on the ground. The GSD is quite smaller on the higher areas, such as the building roofs, but, due to the high flight height, the difference is not so meaningful. The data were acquired by a Zeiss Imaging (Z/I) Digital Mapping Camera (DMC). This is a turnkey, frame-based digital aerial camera system designed to support aerial photogrammetric missions requiring high-resolution and accuracy. The DMC uses eight individual lenses rather than a single lens. The lenses operate simultaneously and collect colour imagery (RGB), CIR (colour infrared), and black-and-white panchromatic imagery. After the flight, the captured image data are

normalized, verified, rectified, colour coded, formatted and made available for digital photogrammetric production.

The first post-processing step is to generate Level 1 images, which include the elimination of defect pixels and a normalization (Diener et al., 2000). Next, the image data are geometrically converted, that is, they are transformed to reduce the perspective distortions, and mosaicked. Finally, the virtual image is generated, and the lens distortions are geometrically corrected, based on the camera calibration. The images created in this way have a new, virtual, camera constant, that is, new independent interior orientation parameters, and can be considered as ideal central perspective photogrammetric images. The employed images were provided with the interior calibration and the external orientation parameters: pose coordinates (X,Y,Z) and attitude (φ,ω,κ). The exterior parameters were calculated during the bundle block adjustment using traditional digital photogrammetric software, which combined the information from the on board sensors (GNSS and IMU) and several Ground Control Points (GCPs) previously measured on the terrain. The DMC images are often available, since they are used for building regional orthophotos, and represent an imaging product covering wide portions of land with a higher detail than satellite images. Therefore, testing a procedure for extracting the currently used geomatics and cartographic products from these images is a great opportunity, notwithstanding some problems to be overcome. The main issue is the management of virtual images in SfM software, which were generally conceived to automatically process simple central-perspective images, with integrated EXIF information.

Since the solar radiation received by the surfaces is strongly influenced by their three-dimensional conformation, a dense Digital Surface Model (DDSM) of the area is needed in order to perform a correct analysis using raster analysis tools in GIS platforms. The processes followed to obtain the most suitable DDSM are summarized in Figure 3.

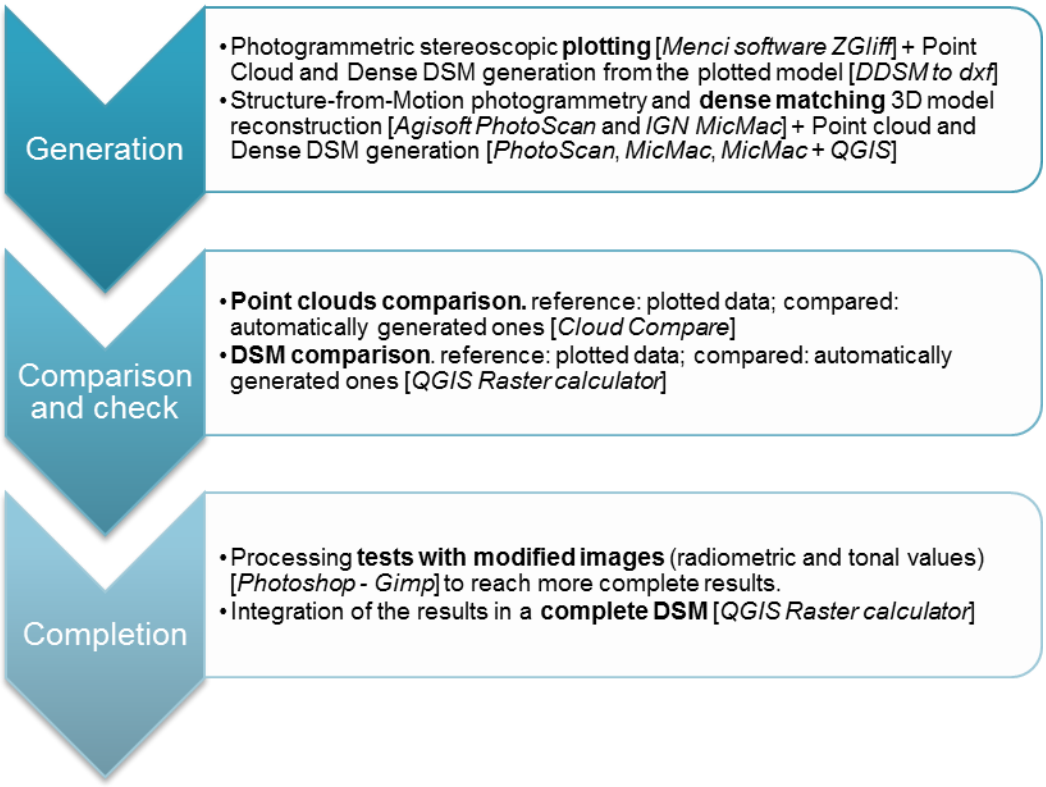

Figure 3: Processing schema for the generation of the dense DSM.

For obtaining a reference product (ground truth), which is useful for checking the reliability of the results processed through an image-matching approach, a traditional stereoscopic plotting was performed using Z-

Map software (www.mencisoftware.it,). This represents a highly controlled 3D drawing of the area, with a very high level of detail, which also offers a better reference than the sometimes available aerial LiDAR data.

For assessing the accuracy of the manual plotting, some empiric rules were applied:

$$\sigma_{XY(nat)} = \sqrt{\sigma^2_{XY(mar)} + \sigma^2_{XY(aim)}}$$

$$\sigma_{Z(nat)} = \sqrt{\sigma^2_{Z(mar)} + \sigma^2_{Z(aim)}}$$

Where:

$\sigma_{XY(mar)}$ = the accuracy of the marked point in XY directions = ±6µm on the image

$\sigma_{Z(mar)}$= the accuracy of the marked point in Z direction = ±0.06 ‰ of the shooting distance

$\sigma_{XY(aim)}$ = the accuracy of the point aimed on the image in XY directions = 7 cm

$\sigma_{Z(aim)}$= the accuracy of the point aimed on the image in Z direction = 8 cm

$\sigma_{XY(nat)}$ and $\sigma_{Z(nat)}$ are the accuracies of the natural points in the final plotted model in the XY and Z directions.

$\sigma_{XY(nat)}$ = 7 cm and $\sigma_{Z(nat)}$ = 9.65 cm

The plotting also avoids neglecting the small geometries of the roofs, such as chimneys or dormers. The plotted model was then converted into a Dense DSM and a dense Point Cloud using a homemade software "DDSM to dxf" (Biasion et al., 2004).

The image-matching methodology was developed and tested for remotely sensed data. It was employed to compute exterior orientation of images in photogrammetry processing and to extract Digital Terrain Model / Digital Surface Model (DTM/DSM) from aerial or satellite stripes (Marr & Hildreth, 1980; Torre & Poggio, 1986; Ackermann, 1984; Baltsavias, 1991). Recently, the methodology has been extensively used in close-range applications concerning architectural and archaeological surveys (Aicardi et al., 2016; Bastonero et al., 2014; Chiabrando et al., 2013; Toldo et al., 2013; Kersten & Lindstaedt, 2012; Remondino & Menna, 2008).

The developed technique was tested here in an urban context. The images were processed automatically using the proprietary low-cost software Agisoft PhotoScan (www.agisoft.ru) and the open source suite Apero–MicMac implemented by IGN (Institut National de l'Information Géographique et Forestière, Paris) (Deseilligny & Cléry, 2011). In both cases, the DMC aerial images and their exterior and interior orientation parameters were used in order to orient the images, to generate the point clouds and the dense DSMs, and, finally, the orthophoto. The data-processing was performed on the total area covered by the images and required a few hours to generate the final results.
In order to perform the image matching, the interior orientation parameters (provided in the calibration certificate) were fixed. This was necessary since the DMC images are provided without any Exif file. The Exif file is usually attached to each digital image, and describes its main details (date and hour when it was shot, image dimensions, used focal length and so on). Such details are read by many photogrammetric and SfM software to obtain parameters useful to initialize the alignment and orientation of the images. In the case

of virtual images deriving from some pre-processing (e.g. the DMC images or spherical images), the virtual geometry does not always enable the correct focal length and distortion parameters to be automatically estimated, since very specific procedures are necessary (Dörstel, 2003). Therefore, the software tools used, at present, cannot automatically calculate the calibration parameters. In particular, Agisoft Photoscan does not work and MicMac calculates a wrong focal length (7.5 mm instead of 120 mm).

For the point cloud and DSM generation, the typical data workflow of this kind of software was followed. In PhotoScan, high resolution "Tie Point Extraction" and "Dense Matching" were set up. As a consequence, a final 65.838.239 point cloud was achieved and subsequently the DSM was generated. In MicMac, using the "Ortho" option in "Malt" (simplified MicMac tool), a dense 50.664.687 point cloud was created. The DSM (stored as integer values to optimize the memory use) were converted into float values (Section 2.1.2) which are useful for data comparison. The results of the adjustments of the two software respect the input exterior orientation values are summarized in Table 1

Table 1: Statistics of the processing results: discrepancies of the exterior orientation values adjusted by the software and the ones provided with the images

	MicMac	**PhotoScan**
Minimum distance [m]	0.711	0.090
Maximum distance [m]	0.766	0.303
Mean distance [m]	0.741	0.165
Standard deviation [m]	0.018	0.032

2.1. Analysis of results and comparisons

The DSMs (grid 20 cm) and the 3D point clouds obtained by the photogrammetry and image matching software tools (MicMac and Photoscan) were compared to the roof shape generated by the manual plotting, in order to evaluate their precision and accuracy. Since these latter data, used as the reliable ground truth, are related to a restricted area of interest, only the image matching results concerning this area were considered, in order to exclude the external parts from the analysis, and thus avoid misleading errors.

2.1.1. *MicMac point cloud vs PhotoScan point cloud*

The comparison between the point clouds was performed using CloudCompare, an OSS that enables 3D models and point clouds to be analysed and measured using several tools (Girardeau-Montaut, 2011). The point to point distances, and thus the discrepancies, between the clouds generated by the SfM software and the reference point cloud, derived from the transformation of the manual plotted model were automatically computed, using the method Nearest Neighbour distance. The statistical results are summarized in Table 2, where the mean value could be considered as representative of the point cloud accuracy, in absence of biases. The gross errors (distance major than 5 m) were removed and not considered for the analysis. However, the point clouds used to perform these analyses are still the complete ones, without any cleaning or filtering, because it was important to evaluate the quality of the entire product; therefore some outliers or noisy objects increase the measured discrepancies to the reference points in some areas. Especially, the higher discrepancies are located on the borders and in correspondence of breaklines. Once the clouds are filtered, eliminating a 20% of these points, the values in Table 3 can be obtained. Table 4 and Figure 4 represent the percentage of points respecting the accuracies (σ) and tolerances (2σ) for a 1:2000 scale. Equally, after a filtering and cleaning process, the percentage of the points included in the tolerance range (0.0 – 0.80 m) increases approximately to the 95%, respecting the validation rules for mapping products.

Table 2: Statistics on the discrepancies between the 3D point clouds produced by MicMac and PhotoScan, without any editing process, and the manually extracted data (as reference).

	MicMac	PhotoScan
Minimum distance [m]	0	0
Maximum distance [m]	2.960	3.687
Mean distance [m]	0.815	0.565
Standard deviation [m]	0.486	0.597

Table 3: Statistics on the discrepancies between the 3D point clouds produced by MicMac and PhotoScan after an editing process, and the manually extracted data (as reference).

	MicMac	PhotoScan
Minimum distance [m]	0	0
Maximum distance [m]	0.901	1.052
Mean distance [m]	0.232	0.196
Standard deviation [m]	0.298	0.301

Table 4: Percentage of points of the generated point clouds respecting the expected accuracies for 1:2000 scale map, derived from the comparison with the reference ground truth (the manually plotted data).

Accuracy range [m]	MicMac	Photoscan
0.0 - 0.40	17.81 %	49.34 %
0.0 - 0.80	57.02 %	83.24 %
0.0 – 1.20	86.17 %	91.31 %

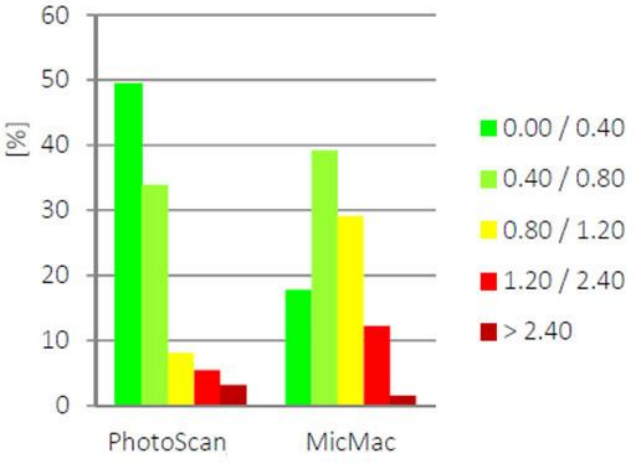

Figure 4 – Cloud to cloud comparison: percentage values distribution

Unfortunately, some points with measured coordinates on the ground, to be used as check points were not available Therefore it was not possible to further assess the quality of the point cloud by means of further statistics and analysis.

2.1.2. MicMac DSM vs PhotoScan DSM

The other analysed products were the DSMs. PhotoScan can easily and automatically provide this data: the algorithm it uses is unknown, however, a high number of scientific researches and tests on cases studies prove its reliability. On the other hand, for MicMac, various intermediate steps are needed. One way is to interpolate the dense point cloud, whose correctness and accuracy were verified beforehand, in GIS software (in this case QGIS with a linear interpolation algorithm was used). Alternatively, a DSM can be built using MicMac (which also uses a linear interpolation). However, for the latter, it is necessary to correct the

generated raster values, since MicMac optimizes the memory by calculating the height raster values using the voxel cell (expressed as height resolution), and establishes an arbitrary height origin, when it produces the TIFF file. This avoids negative values and enables only integer numbers to be managed. The procedure is thus faster and occupies a smaller memory space. This raster therefore had to be transformed into a product to be compared with the other products. The raster calculator tool in QGIS was used, following the relation "(raster value * height resolution) + height origin". The two DSMs were compared to the reference one (derived from the manual plotting) using, again, the QGIS Raster Calculator tools. The differences between the cells in a similar location were computed.

QGIS (www.qgis.org) is a free and OS desktop GIS (subject to the GNU General Public License), which has a user-friendly interface and performs the spatial analysis and processing typical of GIS. It also has some benefits due to the huge number of tools exploitable in the software, fulfilling customized processing needs. The typical QGIS functionalities can be enhanced by other specific python programmed plug-ins, or integrated tool sets from different platforms, such as GRASS (Geographic Resources Analysis Support System) (Neteler et al., 2012), SAGA (System for Automated Geoscientific Analysis), Orfeo Toolbox, and so on.

In order to focus on the surface of the roofs, which were our main interest, some preliminary operations were performed. Only the roofs were extracted by masking the buildings with the areas defined in the Turin digital map (scale 1:2000), using clipping tools in GIS. Since the raw data used to produce the Turin digital map were the same DMC images, with the same parameters, there were no noticeable discrepancies in the superimposition of the two maps. This masking operation was necessary to exclude the areas that could include some misleading statistics, such as the trees along the streets, cars and so on.

Finally, the discrepancies (Figure 5) were calculated through the "Raster Calculator" tool, which makes calculations using raster values. The mean values (Table 5), highlight that the PhotoScan DSM was the nearest to the reference one. The two DSMs derived from the MicMac data show that on most of the surfaces the results were quite similar, but there were problems in areas corresponding to particularly shadowed or dark roofs: these parts were not included in the MicMac DSM. On the other hand, the DSM interpolated in QGIS from the MicMac point cloud presented high errors in those same areas (up to 20 m). We thus chose the DSM produced directly by MicMac, in order to prevent the wrong areas from affecting the further analysis. The final DSMs have a 0.20 m grid.

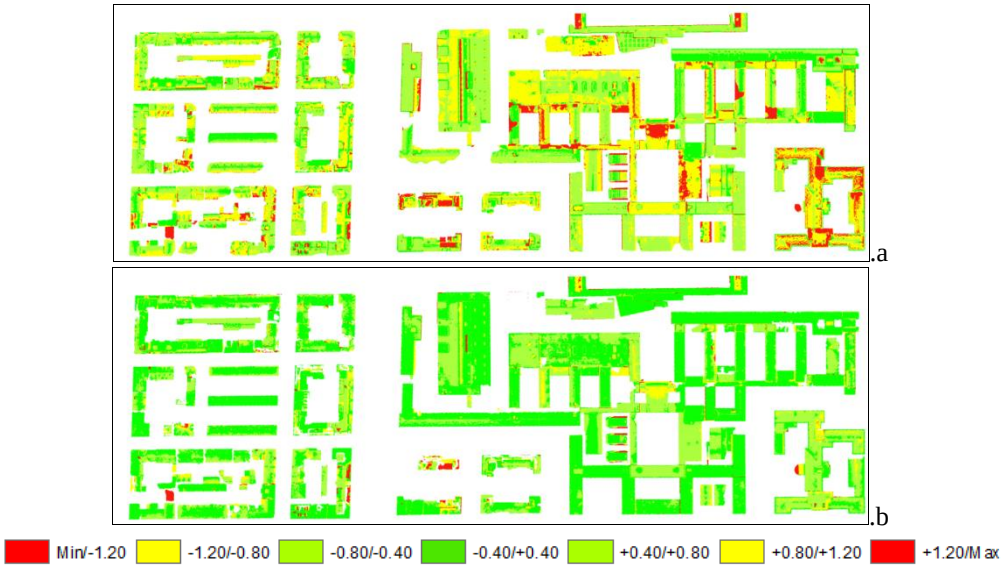

Figure 5: Comparison between DSMs: Manual/MicMac (a) and Manual/PhotoScan (b). The legend is in m.

Table 5: Statistical values of discrepancies between the DSMs and the reference data. The high values in the max cells are due to the outliers distributed on the borders, where the SfM DDSMs are less defined, whereas in the manually plotted DDSM the breaklines are clearly drawn; however mean values respect the required accuracies. The standard deviation values are not reliable, since they are too influenced by the outliers in noisy areas.

	MicMac	MicMac + QGIS	PhotoScan
Minimum distance [m]	0	0	0
Maximum distance [m]	35.095	37.155	35.204
Mean distance [m]	0.593	0.666	0.245
Standard deviation [m]	1.825	3.290	1.228

The generation of the DDSM through the tool "DDSM to dxf", used to convert the 3D plotting into a DDSM and a point cloud, was actually innovative when it was proposed (Biasion et al., 2004), since it allowed the generation of more accurate orthophotos and final cartographic products. Nowadays the use of the SfM software tools seems to be often sufficient to obtain very detailed and defined point clouds and derived products. However, if the images have a low resolution, with high GSD values (as in the DMC images, aiming at 1:10000 representation scale), the number of pixels representing each surface is low and, therefore, the geometry can be not so clear, especially for defining the breaklines of the 3D model. Furthermore, some areas (such as the shadowed or dark areas) have problems when the contrast with neighbouring areas is too high or too low. For these reason it could be a good solution to integrate the two techniques. The SfM algorithms can extract a high number of points for reaching a high level of detail in the reconstructed geometry, also including small details; but for defining some critical breakline or objects which are not sufficiently clear for SfM algorithms, some plotted lines could be fundamental to increase the DDSM quality.

2.2. FILLING THE HOLES

Analysing the completeness of the results, some noisy or missing areas in relation to shadowed zones and dark roofs (Figure 6) were evident. This noise is quite common due to the various factors conditioning the matching process, such as the radiometric quality of the images, image overlapping, shadows and texture (or external features) of the buildings.


a b

Figure 6: Portion of an aerial image (a) with a dark roof (red square) and the lack of relevant information in the generated point cloud (b).

Since the problem could be due to the radiometric and contrast values characterizing the portion of the image (shadowed areas or dark surfaces are affected) (Chiabrando et al., 2014), we completed the model by performing another SfM processing using the same images with modified radiometric and tonal values. In particular, three changes were made to the radiometric values of the original images (in the following identified with "A") using Adobe Photoshop or an OSS alternative such as Gimp:

- conversion into gray scale (B);
- change in tonal values (C);
- conversion into gray scale plus the change in tonal values (D).

We thus reduced the shadowed or dark areas, making them more visible with respect to the background, in order to evaluate the possible improvement in the processed model.

Each set of images was processed separately, following the same workflow explained above. The results were compared, considering both the accuracies of the model, and the completeness of its content. Table 6 shows how the accuracies in the different models are very similar, so that it is possible to consider their integration. Figure 7 indicates the gaps in the different models. Since the gaps are complementary, they can be integrated into a complete model.

Table 6: Statistical values of residuals on 25 check points extracted from the stereoscopic model, for: original images (A), grey scale images (B), modified tonal values (C), grey scale images + modified tonal values (D).

	A	B	C	D
Minimum distance [m]	0.090	0.092	0.091	0.088
Maximum distance [m]	0.315	0.293	0.315	0.290
Mean distance [m]	0.170	0.155	0.174	0.161
Standard deviation [m]	0.068	0.063	0.068	0.062

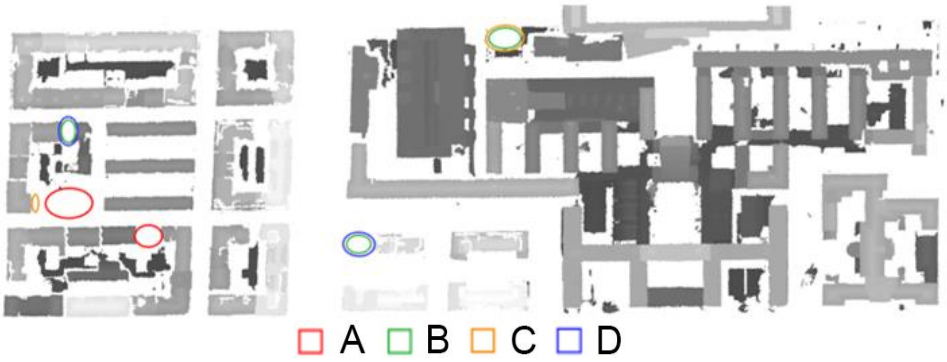

Figure 7: Completeness differences in the DSMs generated from the different sets of images: the circles indicate that the area is present in the model reported in the legend: original images (A), grey scale images (B), modified tonal values (C), grey scale images + modified tonal values (D).

The model derived from the original images was then completed by adding the missing parts from the other models. To perform the integration, various attempts were made considering the point clouds, which are the first generated product, from which the others are derived. However, the best solutions were found by considering the DSMs directly, by integrating the missing parts in the model generated from the original images. This was performed using the Raster Calculator tools in QGIS. In particular, only the roofs were masked and extracted from the various DSMs, and the raster images were integrated in the parts where "no data" value was read in the reference DSM. The complete roofs DSM was thus obtained starting from the available DMC images, without requiring further acquisition phases (Figure 8).

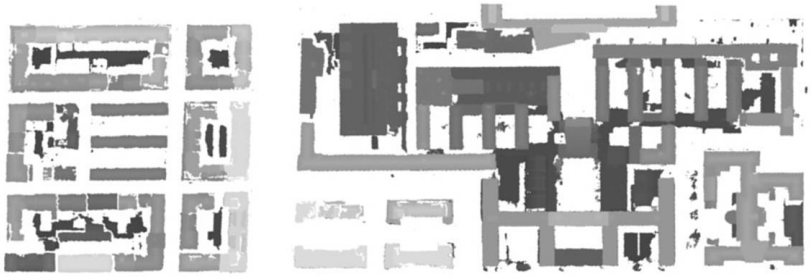

Figure 8: Final integrated DSM.

For this test, Agisoft PhotoScan was used. Similar results, or even better ones, could probably be obtained using MicMac due to the possibility of having more control on the settings in the processing phases.

3. *ANALYSIS OF ROOF SURFACE AND EXTRACTION OF INFORMATION IN GIS*

On the basis of the digital models, by using various tools of the GIS software it is possible to extract information on the solar radiation received by a surface. This is critical information for planning solar panels and system installation. The aforementioned surface analysis processing tools are typical in both proprietary and OS GISs. In this case, QGIS was used again by exploiting the GRASS GIS algorithms, integrated in the QGIS interface. The reliability of the results of the different modules available in GRASS GIS has been tested in a variety of studies (Hofierka & Šuri, 2002; Šuri & Hofierka, 2004). Obviously, the data extracted from the manual DSM are less noisy than the other data, however, if considering the average or median values on homogeneous surfaces, it is possible to verify that the data produced by an image matching approach are compliant with the considered accuracies, and, thus, can be considered reliable.

To perform the analysis of solar irradiation the GRASS tool *r.sun* - solar irradiance and irradiation model, was used. This module calculates five different maps (irradiation layer, insolation time, diffuse irradiation layer, ground reflected irradiation layer, and global irradiance / irradiation layer) in clear-sky conditions, and therefore it does not take into consideration the presence of clouds. The analysis is not only based on the DSM, but is a function of many factors such as aspect, slope, latitude, longitude, declination value, air turbidity coefficients (linke data), and the percentage of diffuse components of the radiation. This information (except for the shadow mask) has to be manually introduced into the shell to run the algorithm. This may be more difficult than a similar process run by other proprietary software, however it enables each step of the processing to be monitored, controlled and customized. Studies have also shown how this software offers more correct and precise results than other proprietary software (Nex et al., 2013). In the analysed case, the processes were performed during the days of the solstice and equinox, and the shadows were incorporated within the results.

Some parts may be difficult for non-expert users, as the plug-ins often need specific formats in input data. For example, the plug-in that computes solar radiation requires the raster maps of the latitudes and longitudes expressed in decimal degrees, however there is currently no specific tool for this task. This requires several steps, each of which needs specific parameters to be set. Therefore, a graphical model was defined through the expressed module in QGIS (http://areeweb.polito.it/geomatics_lab/download/latitute-and-longitude-generation-in-q-gis/). The QGIS graphical model module enables complex models to be defined using a simple interface: the sequence of plug-ins to be run on specific input data can be defined, with pre-set parameters, to obtain the result needed. This saves time and the effort of repeating the same process several times. The model could be enhanced to include full processing (from the DSM to the generation of aspect and slope maps, to the computing of the solar radiation map). This could be useful if these analyses become "good practice" for Public Administrations, which could rapidly obtain useful data.

However, it is useful to consider the approximate errors affecting the slope and aspect maps derived from the DSM processed by MicMac. It is clear, looking at the Figures 9 and 10, that the surfaces of the roof pitches are not smooth, but are affected by some errors. They are due to the many details visible in the images and used to reconstruct the geometry (sometimes a synthesis of a model is necessary, and too many details could give problems in processing some algorithms). Moreover, some areas are affected by noise, which can disturb the model.

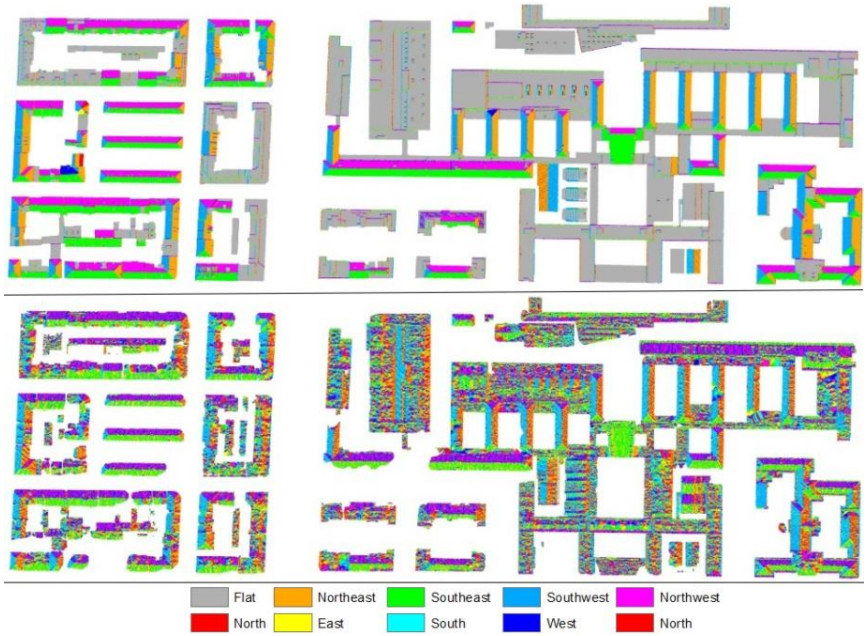

Figure 9: Aspect analysis with manual DSM (upper) and MicMac DSM (lower)

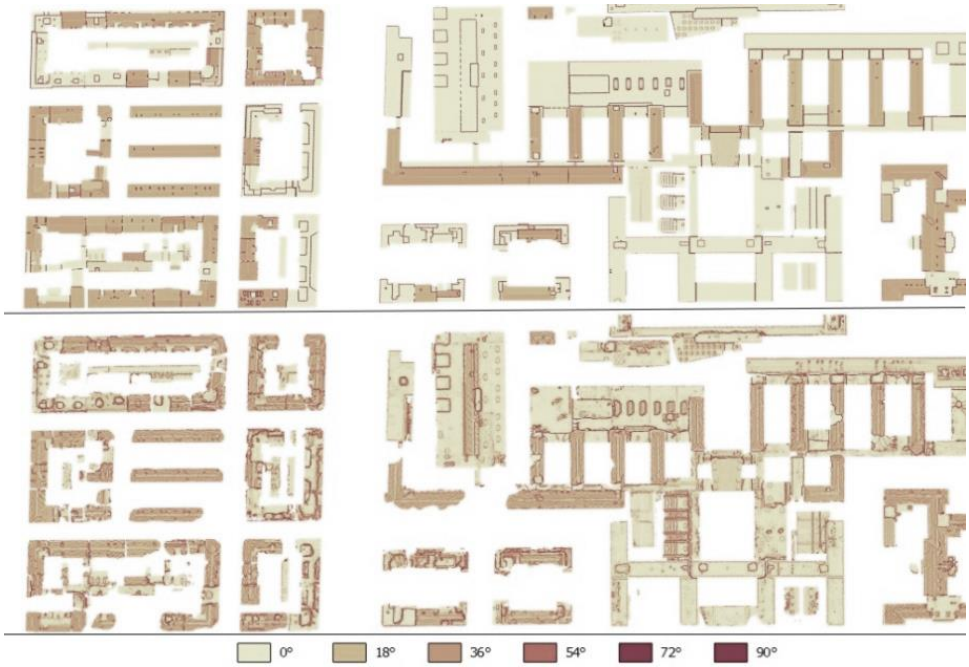

Figure 10: Slope analysis with manual DSM (upper) and MicMac DSM (lower)

The DSM processed through SfM technique was apparently too noisy, compared to the one generated from the manual plotting, so as, consequently, the product generated from it (Figures 11 and 12). For this reason, a deeper test was realized for assessing the reliability of the information extracted from the DSM computed through SfM technique.

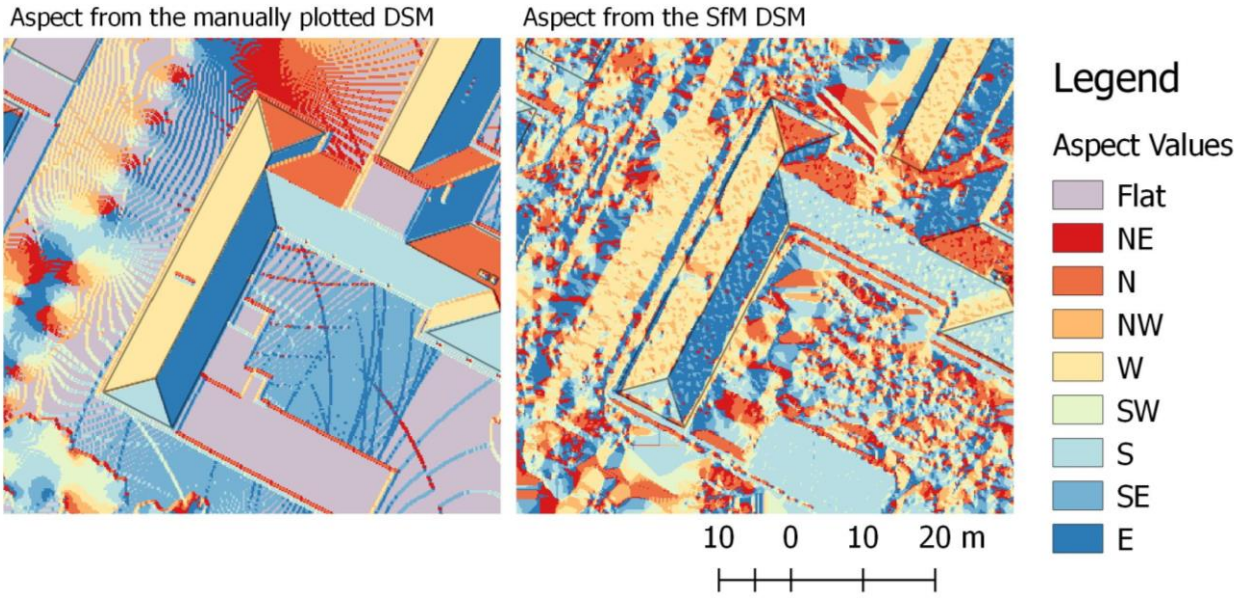

Figure 11 – Raster maps of aspect values generated from the manually plotted DSM and from the SfM DSM. The important object are the roofs, so that the noise outside the roofs area can be ignored, since it is due to other objects present on the ground, vegetation and further interpolation errors where the data are confused.

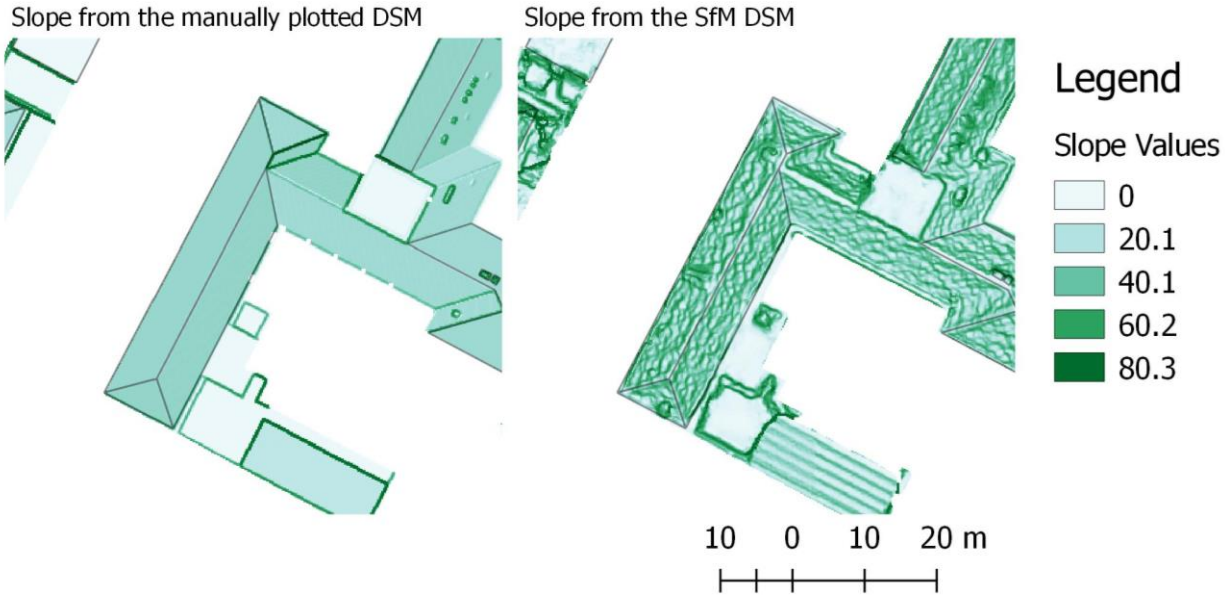

Figure 12 – Raster maps of slope values generated from the manually plotted DSM and from the SfM DSM.

A sample of pitches were considered, oriented in different directions (approximately 20 pitches for each direction, which, in the case study, are north-east, north-west, south-east and south-west). They are visible in Figure 13. Also a sample of flat pitches was investigated, but the results are not here reported because the resulting raster images were too noisy and they presented a number of blunders. Moreover, for evaluating the installation of solar systems on flat roofs it is simply necessary to generate a shadow mask of the area, since the values of solar radiation do not change for the whole area. The values in correspondence of the inclined pitches were considered for performing some statistical analyses on the specific areas. These values and their statistics were computed by means of the "ZonalStatistics" tool in QGIS.

Figure 13 – Map of the roof pitches sample considered for extracting the raster values and performing the analyses.

First of all, the difference between the values of slope and aspect extracted from the two DSMs were compared, since they influence the computation of the solar radiation received by the mapped surfaces. The results are summarized in Table 7. In the Tables 7 and 8 the weighted average on the surface units (the raster pixels) are reported, so that the obtained values are independent from the area of the considered pitches.

Table 7 – Comparison of the values of the slope and aspect raster maps describing the DSM generated from SfM and the ones describing the manually plotted DSM. They are read in correspondence of the pitches samples.

Weighted Average of the discrepancies between the values of the **slope raster of the roofs** generated from the DSM processed through SfM technique and the one extracted from the manually plotted DSM.	**Mean** values [degrees]	3.96
	Median values [degrees]	4.07
Weighted Average of the discrepancies between the values of the **aspect raster of the roofs** generated from the DSM processed through SfM technique and the one extracted from the manually plotted DSM.	**Mean** values [degrees]	20.07
	Median values [degrees]	4.60

For better assessing how much the change in slope and aspect values influence the computation of the final global irradiation, a test was performed using only the DSM extracted from the manual plotting, which presents a more limited noise that possibly affect the results.

Four new raster images were generated from the slope and aspect raster data describing the manually plotted DSM, using the Raster Calculator tool of QGIS:

- A slope raster increased with 5 degrees [function: slope raster + 5] (Slope+5);
- A slope raster decreased of 5 degrees [function: slope raster - 5] (Slope-5);

- An aspect raster increased with 5 degrees [function: aspect raster + 5] (Aspect+5);
- An aspect raster decreased of 5 degrees [function: aspect raster - 5] (Aspect-5).

The value to be added or subtracted (5 degrees) was selected based on the discrepancies of the median values between the manually plotted DSM and the SfM generated one (see Table 7).

These new maps were employed as input to generate new global irradiation maps, which were then compared to the original one (originalGI) to assess how much each parameter influences the processing, and, consequently, what are the tolerances in the slope and aspect values. The global irradiation maps were generated for the day 80 (21st March). For better considering the differences also in the sun position, the different orientations of the pitch surfaces were considered separately. In the studied case, they are: North-East (NE), North-West (NW), South-East (SE) and South-West (SW) (Table 8).

Table 8 – Comparison between the daily sums of solar radiation (global irradiation) values obtained using the original manually plotted DSM (originalGI) and the ones obtained inputting slope and aspect raster maps increased or decreased with 5 degrees. The solar radiation is expressed in kWh/m2/day, and the % values are considered with respect to the average values of the *originalGI*.

		NE		**NW**		**SE**		**SW**	
		[kWh/m^2/day]	[%]	[kWh/m^2/day]	[%]	[kWh/m^2/day]	[%]	[kWh/m^2/day]	[%]
Weighted average of discrepancies between the values of the *originalGI* and the global irradiance raster generated with *Slope+5*	Mean values	4.92	0.15	2.30	0.07	3.23	0.10	3.04	0.09
	Median values	4.64	0.14	1.88	0.06	5.96	0.18	3.32	0.10
Weighted average of discrepancies between the values of the *originalGI* and the global irradiance raster generated with *Slope-5*	Mean values	4.60	0.14	1.54	0.05	7.71	0.24	4.19	0.13
	Median values	5.42	0.17	1.96	0.06	7.30	0.22	4.08	0.13
Weighted average of discrepancies between the values of the *originalGI* and the global irradiance raster generated with *Aspect+5*	Mean values	1.75	0.05	1.64	0.05	9.78	0.30	0.96	0.03
	Median values	1.78	0.05	1.70	0.05	10.44	0.32	1.04	0.03
Weighted average of discrepancies between the values of the *originalGI* and the global irradiance raster generated with *Aspect-5*	Mean values	2.11	0.06	1.61	0.05	9.52	0.29	1.18	0.04
	Median values	2.24	0.07	1.67	0.05	9.84	0.03	1.28	0.04

As it is possible to notice in Table 8, the percentage change is very low (it is always less than 0.5%), as a consequence of the variation of 5 degrees of both slope and aspect. This percentage should be compared with the solar systems efficiency parameters. The tolerance of 5 degrees in the computation of slope and aspect values can be therefore established, and this validates the possibility to employ the DSM generated through SfM technique for performing such kind of analysis supporting the installation of solar systems. Moreover, the computation of solar irradiance is less influenced by the variation of slope in the areas towards the west (less than 0.1%).

Moreover, the discrepancies between the values of global irradiation processed from the manually plotted DSM and the ones derived from the SfM DSM are computed. They are reported in Table 9. Also in this case,

the percentage change is never higher than 0.5%, confirming the results of the previous test, and verifying the possibility to use the SfM extracted DSM for supporting solar systems installation through such analyses in GIS. The apparent noise affecting the DSM does not influence the final results.

Table 9 – Comparison between the daily sums of solar radiation (global irradiation) values obtained using the DSM generated from the manually plotted data and the ones obtained inputting the SfM DSM. The solar radiation is expressed in kWh/m2/day, and the % values are considered with respect to the average values of the manually plotted DSM.

	Weighted average of the discrepancies between the **mean** values of the global irradiance raster of the roofs generated from the DSM processed through SfM technique and the one extracted from the manually plotted DSM.		Weighted average of the discrepancies between the **median** values of the global irradiance raster of the roofs generated from the DSM processed through SfM technique and the one extracted from the manually plotted DSM	
	[kWh/m^2/day]	[% with respect to the average reference values (derived from the manually plotted DSM)]	[kWh/m^2/day]	[% with respect to the average reference values (derived from the manually plotted DSM)]
NE	5.74	0.18 %	3.33	0.10 %
NW	17.07	0.40 %	0.47	0.01 %
SE	15.40	0.25 %	4.29	0.07 %
SW	10.89	0.16 %	8.46	0.12 %

Finally, in order to verify whether the obtained values of solar radiation were reasonable, in terms of numbers and trends, a comparison with the values established by the UNI 10349 (UNI, 2016) for the city of Turin was performed. The UNI 10349 norm is the Italian version of the European standard EN ISO 15927-6:2007 (ISO, 2007), which in turn adopts ISO 15927-6:2007 (Hygrothermal performance of buildings - calculation and presentation of climatic data - Accumulated temperature differences). In the Italian standard, the reference values of solar radiation are reported, together with the procedures to be used in energetic calculations and projects.

For this test, four samples of points with the same aspect values were queried on the generated raster maps (Figure 14). The average of the obtained values was then compared to values stipulated in the norm, as shown in Figure 15. Here, it is clear that the computed geometry is sufficiently reliable to support such kind of analysis about the solar radiation received by the surfaces.

Figure 14: Solar radiation analysis in June. In this analysis, the shadows related to the chimneys or other 3D volumes are considered.

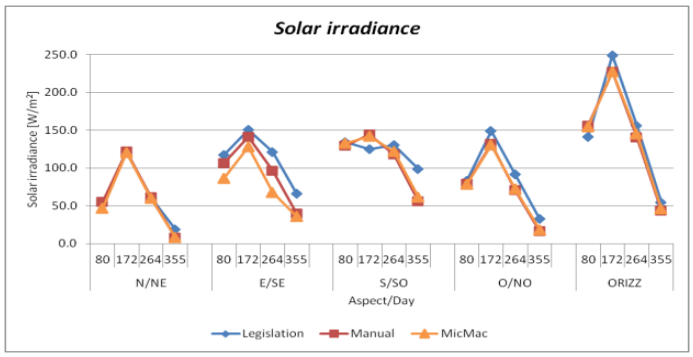

Figure 15: Graph values of the solar radiation in June.

4. CONCLUSIONS

The geometry of the roofs in an area of Turin (Italy) was analysed by means of geomatics methods in order to automatically obtain information for supporting planning of solar systems installation, improving renewable energy exploitation.

The generation of the 3D model was considered, employing digital photogrammetry tools and more automatic SfM software tools, testing also open source software solutions. The 3D model produced by the SfM software (both the OSS MicMac and PhotoScan) result to be accurate enough compared to the data considered as ground truth (the manually plotted data), notwithstanding the higher noise of these products.

Moreover, a deeper analysis of the DSM processed through SfM technique was performed in order to assess the reliability of the computation of solar radiation values generated by the GIS tools starting from these input data. The DDSM generated by SfM is more noisy and, consequently, the slope and aspect raster maps generated from this. On the one hand, this is possibly due to some interpolation procedure or disturbing objects present in the images, and, on the other hand it is too detailed (including, for example some noise due to the irregular surface of the pitches covered with shingles).

Notwithstanding, the statistical analysis on specific characteristics of the DSM (in particular slope and aspect), and a specific test for assessing their tolerance, underlined how the tolerance of 5 degrees (verified in SfM results) can be considered valid and effective for calculating the solar radiation received by the surfaces and consequently supporting solar systems installations.

The proposed expeditious and cost-effective method for analysing the roof pitches to support solar system installation is verified to be reliable and effective.

Non-expert users can exploit the proposed methodology, including the SfM processing of the images and the analysis of the obtained DSM in QGIS (because a graphical model is already proposed here, but other GIS tools and software could be equally effective). Even if some manual operations appears to be essential, a dedicated simple tutorial about the specific operations in the software could be sufficient to guide any user to perform the whole workflow, from the images to the radiation values computation (lasting about 3 hours).

5. *REFERENCES*

Ackermann, F. (1984). Digital image correlation: performance and potential application in Photogrammetry. The Photogrammetric Record, 11(64), 429–439.

Agenzia per l'Italia Digitale– Presidenza del Consiglio dei Ministri (2013), Circolare 6 dicembre 2013 n.63 - *Linee guida per la valutazione comparativa prevista dall'art. 68 del D.Lgs. 7 marzo 2005 n. 82 "Codice dell'amministrazione digitale".*

Agugiaro, G., Nex, F., Remondino, F.,De Filippi, R., Droghetti, S., and Furlanello, C. (2012). Solar radiation estimation on building roofs and web-based solar cadastre. *ISPRS Annals of the Photogrammetry, Remote Sensing and Spatial Information Sciences*, I-2, pp. 177-182. XXII ISPRS Congress.

Aicardi, I., Chiabrando, F., Grasso, N., Lingua, A.M., Noardo, F., Spanò, A. (2016). UAV photogrammetry with oblique images: first analysis on data acquisition and processing. *ISPRS International Archives Of The Photogrammetry, Remote Sensing And Spatial Information Sciences 2016*. Scopus: 2-s2.0-84987899476 doi: 10.5194/isprsarchives-XLI-B1-835-2016.

Baltsavias, E. P. (1991). Geometrically constrained multiphoto matching, *Mitteilungen*, 49, Swiss Federal Institute of Technology (ETH), Zürich, Switzerland.

Borfecchia, F., Pollino, M., De Cecco, L., Martini, S., La Porta, L., Marucci, A., and Caiaffa, E. (2013). Integrated GIS and Remote Sensing Techniques to Support PV Potential Assessment of Roofs in Urban Areas. Computational Science and Its Applications – ICCSA 2013, pp. 422-437.

Brovelli M.A., Cina A., Crespi M., Lingua A.M., and Manzino A. (2010). *Ortoimmagini e modelli altimetrici a grande scala – Linee guida*, CISIS.

Bastonero, P., Donadio, E., Chiabrando, F., and Spanò, A. (2014). Fusion of 3D models derived from TLS and image-based techniques for CH enhanced documentation. *ISPRS Annals Of The Photogrammetry, Remote Sensing And Spatial Information Sciences*, 2, pp. 73-80.

Chiabrando, F., Lingua, A., Noardo, F., and Spanò, A. (2014). 3D modelling of trompe l'oeil decorated vaults using dense matching techniques. *ISPRS Annals of the photogrammetry, remote sensing and spatial information sciences*, 2, pp. 97-104.

Chiabrando, F., Lingua, A., Piras, M. (2013). Direct photogrammetry using UAV: tests and first results. *ISPRS Archives of the photogrammetry, remote sensing and spatial information sciences*, XL-1, W2, UAV-g2013, Rostock, 4–6 September 2013, pp. 81-86. ISSN: 2194-9034.

Deseilligny, M. P., and Clery, I. (2011). Apero, an open source bundle adjusment software for automatic calibration and orientation of set of images. *ISPRS-International Archives of the Photogrammetry, Remote Sensing and Spatial Information Sciences*, 38, 5.

Diener, S., Kiefner, M., and Dörstel, C. (2000). Radiometric normalisation and colour composite generation of the DMC. *International Archives of Photogrammetry and Remote Sensing*, XXXIII, Part B1, pp. 82-88.

Dörstel, C. (2003). DMC-Practical Experiences and Photogrammetric System Performance. In: Fritsch D.(Ed.), *Photogrammetric Week 2003*.

Girardeau-Montaut, D. (2011). *CloudCompare-Open Source project*.

Hofierka, J., Kaòuk J., and Gallay, M. (2014). "The spatial distribution of photovoltaic power plants in relation to solar resource potential: the case of the Czech republic and Slovakia". *Moravian Geographical Reports*, n. 2/2014, 22, pp.26-33.

Hofierka, J., and Šuri, M. (2002). The solar radiation model for Open source GIS: implementation and applications. *Proceedings of the Open source GIS - GRASS users conference*, pp. 1-19.

Kersten, T. P., and Lindstaedt, M. (2012). Automatic 3D object reconstruction from multiple images for architectural, cultural heritage and archaeological applications using open-source software and web services. *Photogrammetrie – Fernerkundung - Geoinformation, 2012*(6), pp. 727-740.

Biasion A.; Dequal S.; Lingua A., (2004) A new procedure for the automatic production of true orthophotos, *International Archives of the Photogrammetry, Remote Sensing and Spatial Information Sciences*, 35(B4).

Marr, D., and Hildreth, E. (1980). Theory of edge detection. *Proceedings of the Royal Society of London. Series B, Biological Sciences.* 207(1167), pp. 187-217.

Neteler, M., Bowman, M.H., Landa, M., Metz, M. (2012). GRASS GIS: A multi-purpose open source GIS. *Enviromental Modelling & Software*, 31, Maggio 2012, pp. 124-130.

Nex, F., Remondino, F., Agugiaro, G., De Filippi, R., Poletti, M., Furlanello, C., Menegon, S., Dallago, G., and Fontanari, S. (2013). 3D SolarWeb: a solar cadaster in the Italian alpine landscape. *International Archives of the Photogrammetry, Remote Sensing and Spatial Information Sciences*, XL-7/W2.

Remondino, F., and Menna, F. (2008). Image-Based surface measurement for close-range heritage documentation. *International Archives of Photogrammetry, Remote Sensing and Spatial Information Sciences.* XXXVII, part B5-1, pp. 199-206.

Šuri, M., and Hofierka, J. (2004). A New GIS-based solar radiation model and its application to photovoltaic assessments. Transactions in GIS, 8, pp. 175-190.

Toldo, R., Fantini, F., Giona, L., Fantoni, S., and Fusiello, A. (2013). Accurate multiview stereo reconstruction with fast visibility integration and tight disparity bounding. *International Archives of Photogrammetry, Remote Sensing and Spatial Information Sciences*, 40(5/W1), pp. 243–249.

Torre, V., and Poggio, T. A. (1986). On edge detection. Pattern Analysis and Machine Intelligence, *IEEE Transactions on*, (2), pp. 147-163.

UNI (2016). *UNI 10349, Riscaldamento e raffrescamento degli edifici – Dati climatici*.

ISO (2007). ISO 15927-6:2007, *Hygrothermal performance of buildings -- Calculation and presentation of climatic data Accumulated temperature differences.*